ACS APPLIED MATERIALS & INTERFACES

Research Article

www.acsami.org

Synergistic Effect of Hybrid Carbon Nanotube–Graphene Oxide as Nanoadditive Enhancing the Frictional Properties of Ionic Liquids in High Vacuum

Lili Zhang,[†,‡] Jibin Pu,[†] Liping Wang,*[,†] and Qunji Xue[†]

[†]State Key Laboratory of Solid Lubrication, Lanzhou Institute of Chemical Physics, Chinese Academy of Sciences, No. 18, Tianshui Middle Road, Lanzhou 730000, P. R. China

[‡]University of Chinese Academy of Sciences, Beijing 100039, P. R. China

Supporting Information

ABSTRACT: A remarkable synergetic effect between the graphene oxide (GO) layers and multiwalled carbon nanotubes (MWCNTs) in improving friction and wear on sliding diamond-like carbon (DLC) surfaces under high vacuum condition (10^{-5} Pa) and low or high applied load is demonstrated. In tests with sliding DLC surfaces, ionic liquid solution that contains small amounts of GO and MWCNTs exhibited the lowest specific friction coefficient and wear rate under all of the sliding conditions. Optical microscope images of the wear scar of a steel ball showed that GO/MWCNT composites exhibited higher antiwear capability than individual MWCNTs and GO did. Transmission electron microscopy images of nanoadditives after friction testing showed that MWCNTs support the GO layers like pillars and prevent assembly between the GO layers. Their synergistic effect considerably enhances IL-GO/MWCNT composites.

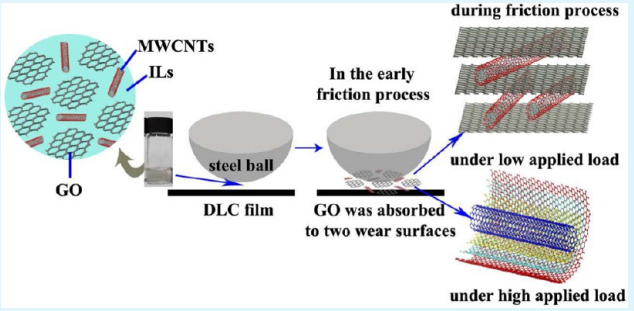

KEYWORDS: *ionic liquids, vacuum, graphene oxide, multiwalled carbon nanotubes, synergistic effect, nanoadditive, tribology*

1. INTRODUCTION

The demand for lubricants and lubrication system in outer space is different from that for applications on the ground. The space environment of high vacuum, microgravity, strong radiation, and extreme temperature warrants new requirements for lubricants and lubrication systems.[1] Many studies have revealed the advantages of diamond-like carbon (DLC) coatings and the unique properties of space liquid lubricants. A new type of solid–liquid composite coating that consists of DLC and ionic liquids (ILs) for space applications has been developed to improve durability and reliability of DLC coatings. DLC/IL composite coatings exhibit satisfactory friction performance in simulated space environments.[2] However, friction coefficients and wear rates of DLC/IL coatings under high vacuum conditions remain high, particularly at the running-in stage. In a comparison with the properties of oil lubricants, lubricants consisting of additives enhance friction-reducing and antiwear properties and prevent lubricant degradation and corrosion in mechanical systems.[3−8] For instance, M. Ratoi compared the friction, wear, and micromechanical properties of WS_2 with zincdialkyldithiophosphate (ZDDP) and ZDDP–organic friction modifier (OFM) mixture.[9] WS_2 generated tribofilms much faster than ZDDP + OFM, and these showed a superior ability to decrease the friction in the boundary regime. Vijaykumar et al. examined the tribological behavior of copper oxide nanoparticles as additives in mineral-based multigrade engine oil.[10] The results demonstrated that nanoparticle additives can effectively improve the engine oil lubricating properties. They convert sliding friction into rolling friction, thus reducing the effective friction coefficient. A similar study was also reported: Exceptionally stable CuO particles coated with sodium oleate (SOA) were used as a nanoparticle additive in base oil with no other additives.[11] It is observed that CuO/SOA nanoparticle additives reduce the friction between the lubricated surfaces in the absence of any other conventional additives. The effect of nanoparticles is more influential at higher loads and concentrations. Also, the steady state temperature is also 10 °C lower on average for nanolubricants.

Graphene is pure carbon in the form of a one-atom-thick, nearly transparent sheet. Given its high load-bearing capacity, high chemical stability, and weak intermolecular and strong intramolecular forces, graphene has received considerable attention in the field of tribology. In particular, graphene additives markedly improve friction coefficient and antiwear under boundary lubrication conditions. For example, previous studies investigated the tribological properties of graphene layers, which serve as additives to liquid lubricants; their results showed that graphene layers can decrease the friction

Received: January 20, 2015
Accepted: March 31, 2015
Published: March 31, 2015

DOI: 10.1021/acsami.5b00598
ACS Appl. Mater. Interfaces 2015, 7, 8592–8600

coefficient and wear under proper conditions. Their antiwear and reduced friction mechanisms were also discussed, and an in situ solid film deposition mechanism was proposed.[12] Varsha Khare studied the potential of a graphene−IL hybrid nanomaterial for engineering applications with a focus on "lubricant" properties to reduce frictional forces to enhance friction performance.[13] These researchers find that reduction in friction coefficient of three lubricant systems occurs via different mechanisms as predicted by microscopy imaging. One explanation is that graphene layers can separate two contact surfaces.

Graphene is not soluble or dispersible in most solvents because of its chemical inertness. Graphene oxide (GO) consists of a 2D sheet of covalently bonded carbon atoms that bear various oxygen functional groups (e.g., hydroxyl, epoxy, and carbonyl groups) on their basal planes and edges, which confer GO layers partial hydrophilicity and thus high stability in aqueous medium.[14] Uniform dispersion without any agglomeration of the GO in the base oil can be obtained by maximizing the surface −OH and −COOH introduced during the GO preparation. A functionalization with long chain compounds (i.e., aliphatic amine to obtain the amide derivative) enhances dispersion in nonpolar solvents.

However, the large surface area between a few graphene layers results in large van der Waals forces and strong interactions.[15] Thus, the performance of graphene-based oil is limited by the aggregation and stacking of graphene sheets. Graphene sheets stack on each other and show no effective uniform coverage on the tribofilm surface; thus, the performance of graphene sheets significantly suffers. Nanomaterials, particularly carbon nanotubes (CNTs), can effectively prevent GO or graphene from restacking and also reinforce their electrical conductivity, ion diffusion, and electrochemical character. CNT-GO hybrids have been employed as reinforcing and functional fillers in polymer composites.[16−20] Composite materials filled with CNT-graphene hybrids possess high electrical conductivities and excellent thermal and mechanical properties. It was also reported that the performance of composite additives was better than that of a single additive. Altavilla et al. reported a new kind of hybrid organic−inorganic nanocomposite, which consisted of an inorganic core of CNT/MoS_2 coaxial nanotubes coated by oleylamine molecules. This kind of hybrid nanostructure conjugates and enhances, through a unique synergy, the performances of CNTs and nanochalcogenides with an organic coating that promotes the compatibility in nonpolar matrix (solvent, oil, grease).[21] Introduction of CNTs may effectively prevent GO from restacking while reducing friction. Material and morphology of nanoparticles have a crucial effect on both the wear and the coefficient of friction, primarily by affecting their macroscopic hardness, as well as the thickness and the surface coverage of their transfer films.[22] We previously compared the tribological properties of graphene and multiwalled CNTs (MWCNTs) as oil additives and found that MWCNTs and graphene layers can effectively improve the performance of ILs in low and high load conditions, respectively. In the present study, we integrate GO and MWCNTs into ILs and prepare DLC/IL/(GO-MWCNT) coatings that exhibit friction-reducing and wear-resistance properties in high vacuum conditions. The introduction of MWCNTs can also effectively prevent GO from restacking while reducing friction.[23]

2. EXPERIMENTAL SECTION

2.1. Materials. The IL 1-butyl-3-methylimidazolium tetrafluoroborate (purity, 97%) was prepared as previously described.[24,25] Powders of multilayer GO were purchased from Nanjing XFNANO Materials Tech Co., Ltd. MWCNTs were sectioned as previously described.[26,27]

2.2. Preparation of Nanofluids and Hybrid Films. The optimum graphene concentration (0.075 mg mL^{-1}) obtained by previous screen test[28] was adopted for the additives in the test. The dispersions were prepared as follows: GO, MWCNTs, and their mixtures, with different mass ratios of GO to MWCNTs (30:70, 50:50, and 70:30), were separately dispersed into ILs through ultrasonication for 2 h to obtain a series of homogeneous and dark suspensions (0.075 mg mL^{-1}). The pure ILs, ILs with GO or MWCNTs, and ILs with different mass ratios of GO to MWCNTs were abbreviated as ILs, IL-GO, IL-MWCNTs, IL-GO30, IL-GO50, and IL-GO70, respectively. The resulting nanofluids were coated on DLC films by spinning at 2000 rpm for 30 s. The thickness of the resulting nanofluid layer was approximately 0.5 mm. The interaction between the solid DLC film and the upper liquid film was mainly physical adsorption. Finally, the hybrid coatings were formed on DLC film for friction experiments under a high vacuum condition.

2.3. Friction Tests. All friction tests were conducted on the same self-made rotational ball-on-disk vacuum tribometer in high vacuum (10^{-5} Pa). Commercially available steel balls (AISI-52100) with a diameter of 3 mm were used as the counterparts. Sliding experiments were performed with a normal pressure varying from 10 to 30 N and a sliding velocity ranging from 0.021 to 0.26 m s^{-1}. Each friction test was 60 min, and the friction coefficient was recorded as the average value in the steady state.

2.4. Characterization. The GO and MWCNTs were characterized using high resolution transmission electron microscopy (FEI Tecnai F300). The ILs, IL-GO, IL-MWCNTs, GO, and MWCNTs were characterized by using a thermogravimetric analyzer (TGA-7, PerkinElmer) in flowing N_2. The ILs, IL-GO, and IL-MWCNTs were characterized by using a UV−vis spectrophotometer (HP8453, Agilent/HP). The contact angles of the samples were measured with a Krüss-DSA100 at room temperature. The wear scar diameters on the steel balls were measured using an optical microscope (STM6, Olympus), and the worn surface of the balls after the friction testing was characterized by Raman spectroscopy (Lab RAM HR800, with 532 nm laser excitation). The wear depth and wear track profiles after the friction tests were obtained by a noncontact 3D surface profiler (model Micro MAXTM, ADE Phase Shift, Tucson, AZ), and the disc wear rate was calculated from the wear depth. The changes in chemical composition of the nanofluids were investigated via X-ray photoelectron spectrometer (XPS, ESCALAB 250Xi, Thermo-Fisher Scientific), and surface analysis was performed on the disk surface after sliding tests using time-of-flight secondary ion mass spectroscopy (TOF-SIMS, ION TOF-SIMS IV). The TOF-SIMS testing specimens after the friction test were ultrasonically cleaned with acetone for 10 min. The viscosities of the ILs and nanofluids were measured by using a Stabinger viscometer (SYP1003-III, Anton Paar).

3. RESULTS AND DISCUSSION

3.1. Physical and Chemical Properties. For tribology applications in space, the wettability of the nanofluids was investigated. The contact angles of the five nanofluids are very close to those of ILs (69.7°), in the range 69.5−71.5°, indicating that the wettability of ILs is not affected by the addition of GO and MWCNTs. The contact angles were summarized in Table S1, Supporting Information. Our UV−vis spectrophometric measurement can easily characterize quantitatively and accurately the stability of the MWCNTs and GO dispersion. The UV−vis absorption spectra of the IL dispersions of GO and MWCNTs are shown in Supporting Information Figure S2. No noticeable changes can be observed in the MWCNTs and GO dispersion before and after 1 week of placement. TGA curves were analyzed to estimate the thermal stability of the nanofluids. The result is shown in Figure S3, Supporting Information.

DOI: 10.1021/acsami.5b00598
ACS Appl. Mater. Interfaces 2015, 7, 8592−8600

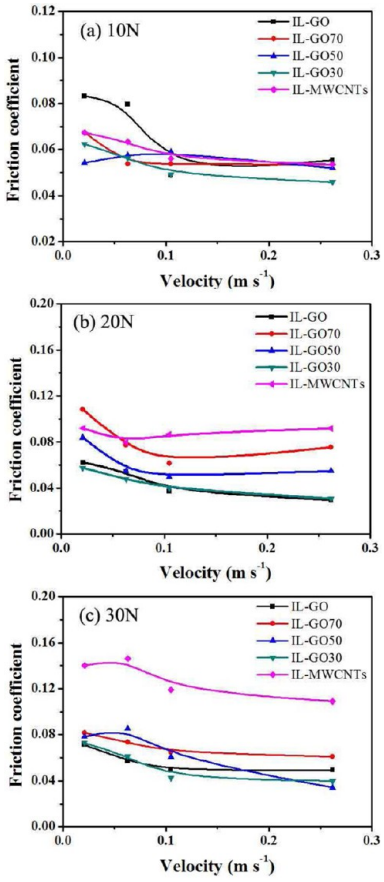

Figure 1. Variations in friction coefficient of ILs, IL-MWCNTs, IL-GO, IL-GO30, IL-GO50, and IL-GO70 under different velocities: (a) 10, (b) 20, and (c) 30 N.

3.2. Tribological Characterization. Figures 1−3 summarize the friction and wear results of IL-GO/MWCNT composites under different sliding conditions, compared with those of IL-GO and IL-MWCNTs. As shown in Figure 1, the tribological properties of IL-GO and IL-MWCNTs clearly depend on the load. IL-MWCNTs exhibit a low friction coefficient at an applied load of 10 N, whereas IL-GO has a low friction coefficient at applied loads of 20 and 30 N. In particular, IL-GO30 displays the lowest specific friction coefficient and wear rate under all of the sliding conditions. As seen from the noncontact 3D surface profiler images and cross-section profiles of the wear tracks at different loads in Figures 2 and 3, IL-GO/MWCNT (IL-GO30) composites exhibited shallower wear tracks than individual IL-MWCNTs and IL-GO did. These data suggest that the tribological performance of the IL-GO/MWCNT composites is better than that of a single IL-GO or IL-MWCNTs.

This performance can be described as the lubrication regime transition.[29] Nanoadditives affect the viscosity of ILs, which can influence the film thickness between two sliding surfaces. According to Hamrock−Dowson (H−D) theory,[30,31] the film thickness of IL, IL-MWCNT, IL-GO, and IL-GO30 solutions can be predicted by the following expression

$$H_c^* = 2.69\frac{G^{*0.5}3u^{*0.67}}{W^{*0.067}}(1 - 0.61e^{-0.73k}) \quad (1)$$

where $H_c^* = h_c/R$, $G^* = \alpha E'$, $u^* = \eta_o u/E'R$, $W^* = W/E'R^2$, h_c is the film thickness, R is the radius of the ball, α is the pressure-viscosity coefficient of the ILs ($\alpha = 9.9 \times 10^{-9}$ Pa^{-1}),[32] u is the average linear speed of a glass plate and ball, W is the load, k is a coefficient (~1), and E' is the reduced Young's modulus of the two contacting solids defined by

$$E' = \left(\frac{1 - \upsilon_1^2}{E_1}\right)\left(\frac{1 - \upsilon_1^2}{E_2}\right) \quad (2)$$

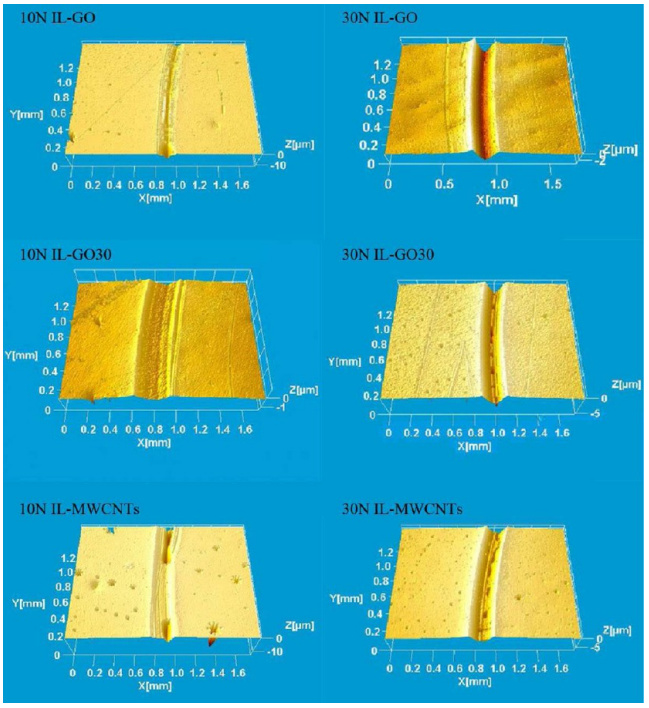

Figure 2. Noncontact 3D surface profiler images of DLC/IL/GO-MWCNT film after friction testing.

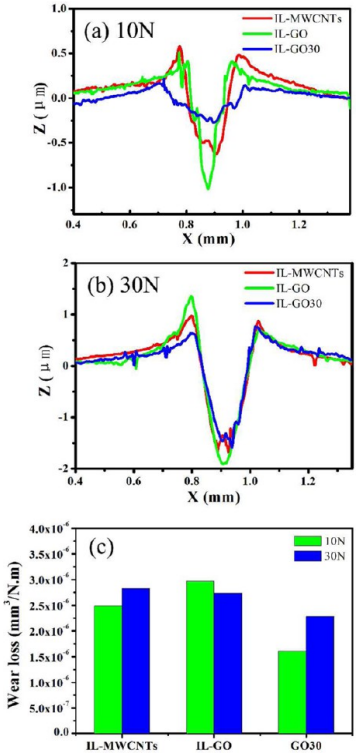

Figure 3. Disc wear rates and cross-section profiles of the wear tracks at different loads.

DOI: 10.1021/acsami.5b00598
ACS Appl. Mater. Interfaces 2015, 7, 8592−8600

Here, ν_i is Poisson's ratio for material i, E_i is the elasticity modulus of material i, and η_o is the viscosity of ILs and nanofluids. The film thickness between two surfaces as a function of oil with and without nanoadditives, predicted by the H−D equation, is shown in Figure 4. The corresponding

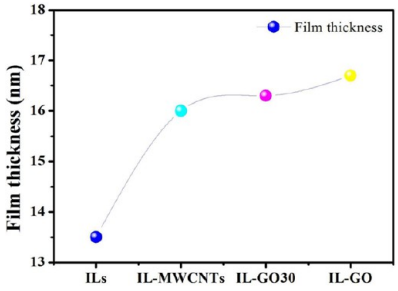

Figure 4. Film thickness under the lubrication of ILs and nanofluids predicted by the H−D equation.

lubrication regime can be approximately predicted according to the ratio of h_c/R_a,[29] where h_c is the thickness of the lubrication film and R_a is the roughness of the solid surface. Due to the point of contact at a high load, the lubrication in ILs belongs to the mixed lubrication regime that contains dry contact and boundary lubrication. The viscosity of nanofluids increases the thickness of the lubrication film, consequently increasing h_c/R_a. Thus, the lubrication proceeds into the boundary lubrication regime.

3.3. Surface Analysis. XPS analysis was used to further clarify the chemical states of the typical elements of oils on the wear scar. As shown in Figure 5a, the C 1s peak of

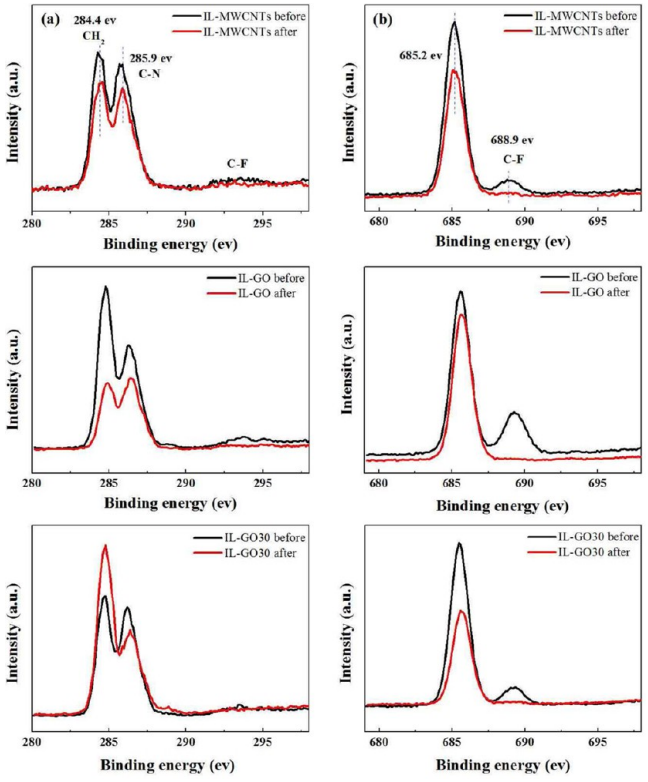

Figure 5. XPS spectra of nanofluids before and after friction testing: (a) C 1s spectra, (b) F 1s spectra.

IL-MWCNTs before friction testing shows three peaks at 284.8, 285.9, and 292−296 eV, which correspond to CH_2, C−N, and C−F, respectively. It was indicated that some of the C atoms and F atoms formed weak bonds and generated CF_2 groups during sonication. The prominent F peak at 688.9 eV after friction testing is additional evidence of C−F bonds. With only a few F atoms forming weak bonds with C atoms during sonication, the C−F peak intensity in the C 1s spectrum is considerably weakened to the point that it is nearly invisible. The C−F peak intensity of both nanofluids becomes weaker compared with that of the peak in low binding energy, which is attributed to Fe−F and B−F bond formation after friction testing. A possible reason for this phenomenon is that more F atoms form strong bonds with Fe atoms originating from the wear debris of the steel ball. The Fe 2p peak at 710−715 eV also supports the existence of FeF_2 and FeF_3.[33,34] Figure 6

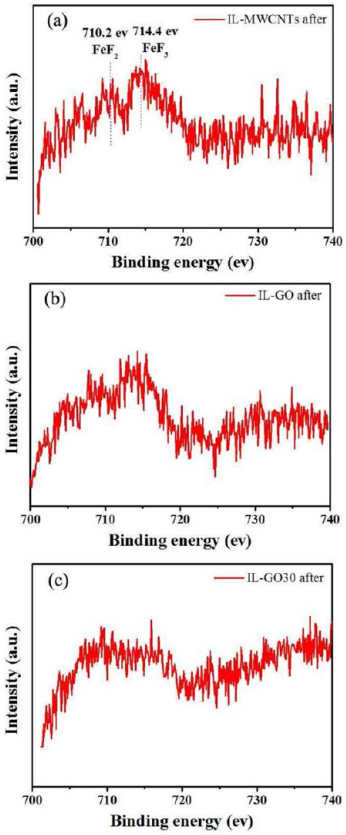

Figure 6. XPS spectra of nanofluids before and after friction testing: Fe 2p spectra for (a) IL-MWCNTs, (b) IL-GO, and (c) IL-GO30.

shows the XPS peaks of the Fe 2p spectrum appearing at 710.2 and 714.4 eV, which corresponds to FeF_2 or FeF_3. On the basis of the results of XPS analysis, it is deduced that tribochemical reaction products were mainly composed of FeF_2 and FeF_3.

For the obervation of obvious tribochemical reaction of ILs, steel ball sliding against steel under lubrication of ILs was investigated in high vacuum. Chemical composition in the worn surface was obtained by the TOF-SIMS analysis. Analyses of ILs with respect to the cation, anion, and F (elements of anion) detected the count ratio. The cation count ratio inside the sliding track was smaller than that outside the sliding track (see in Figure 7). The anion and F count ratios inside the sliding track increased compared to those measured outside. So, major components in the worn surface are the elements derived from

DOI: 10.1021/acsami.5b00598
ACS Appl. Mater. Interfaces 2015, 7, 8592−8600

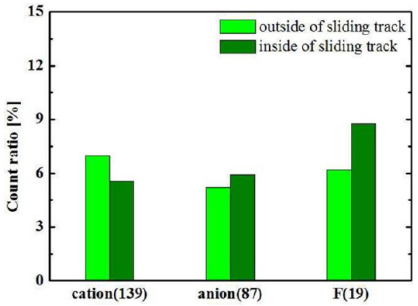

Figure 7. Count ratio by the TOF-SIMS analysis using ILs.

the anionic moiety. Also, a chemical image in the worn surface is shown in Figure 8. The analyzed area is marked in Figure 8a. The worn surface of ILs consists of two typical areas, namely, the "inner area" and the "outside area". Figure 8b–f shows a chemical image of these analyzed areas. Contents of the elements in the chemical image are expressed by contrast. A bright area indicates a higher concentration of the focused element. In Figure 8c, the inner area gets darker than the outside area, because the F anion reacted with Fe, which was generated by decomposition of the BF_4 anion and generated Fe–F compounds. Correspondingly, as shown in Figure 8e,f, FeF_3^- and FeF_2^- were detected from the inner area lubricated by a BF_4 anion. So, the anion reacted with or adsorbed on the sliding surface.

3.4. Microscopic Observations. Such outstanding enhancement of IL-GO/MWCNT composites can be principally attributed to their synergistic effect. The following sections further discuss the corresponding GO/MWCNT-related mechanisms on the basis of the microscopic observations of worn surfaces and counter-faces.

As shown in Figure 9a,c, the wear scar diameters of steel balls are approximately 222 and 236 μm after sliding against the steel balls. However, the wear scar diameter of the ball using IL-GO/MWCNT (IL-GO30) composites is reduced to ~213 μm (Figure 9b). The optical micrograph of the steel ball shows dark patches that cover the track area. The corresponding Raman spectra of the wear scar (Figure 9d–f; the D-band at ~1357 cm^{-1} and G-band at ~1591 cm^{-1} are ascribed to carbon) confirm the presence of nanocarbon film and deposit on the steel ball.

Moreover, with the addition of MWCNTs to the ILs, the MWCNTs have acquired defects during the sliding tests under high applied load, as evidenced from the increase in D peak intensity (I_D/I_G) from 1.10 of IL-MWCNTs before friction testing to 1.52 after friction testing. This variation suggests that in-plane defect concentration is increased in the MWCNTs during friction testing. We selected IL-MWCNTs and IL-GO after friction testing (30 N) to dilute in alcohol by ultrasonic dispersion for a long time and carry out the TEM of MWCNTs and GO. Figure 10a presents the TEM image of GO after friction testing. It is easy to see that additional layers with a different orientation stacked on the GO nanosheets. GO layers significantly become thicker due to overlapping after friction testing. For use in the MWCNTs, carbon nanotubes intertwine with one another. Wear debris or graphene-like lamellas are observed together with MWCNTs that are likely generated by friction. It can be indicated that more wear debris appears for no early GO transfer layer.

IL-GO30 (30 N) was also observed by TEM. Clearly, the graphene layers are peeled off from the MWCNTs in Figure 11a; other examples are presented in Figure 11b,c. Figure 11b shows that the graphene sheets left the parent MWCNTs. Figure 11c shows that the left graphene sheets from the MWCNTs have been absorbed into the graphene nanosheets. In addition, Figure 11b shows that the MWCNTs disperse between the GO layers and that GO represents a typical wrinkled morphology. Meanwhile, GO looks thicker with fewer MWCNTs in the area, and then the typical wrinkled morphology disappears. In Figure 11d, a good distribution of the MWCNTs was also observed on the surface of the graphene platelets which act as a spacer for GO. Fewer adsorbed MWCNTs are present on the thicker GO layers. In a comparison with nanoadditives under low applied load (Figure 12), a similar structure can be observed. MWCNTs are sandwiched between the GO sheets, but a fairly complete hollow structure still remains after low applied load friction testing. Our previous research revealed that graphene thickens after a long friction time.[35] We believe that the existence of MWCNTs can effectively prevent two or more layers of graphene from aggregating to form thick layers.

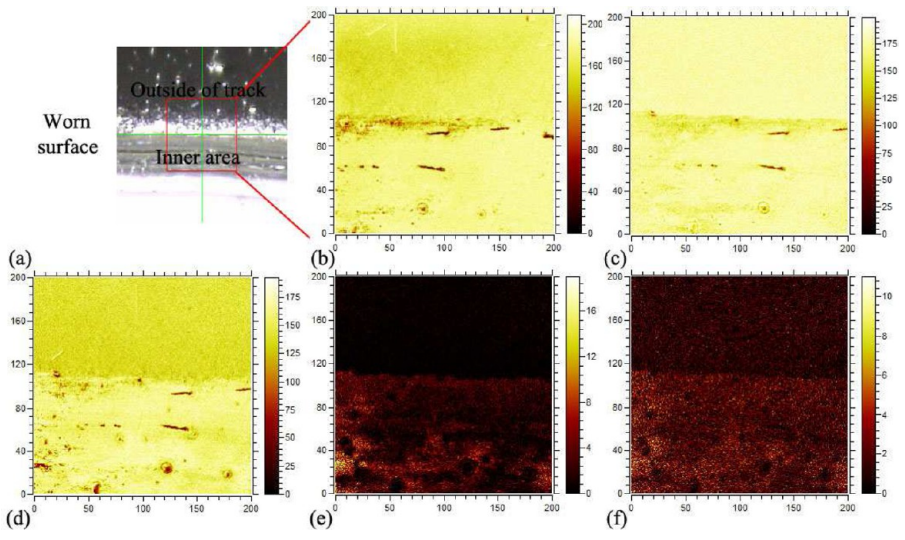

Figure 8. TOF-SIMS image of worn surface lubricated by ILs: (a) analyzed area, (b) $C_8H_{15}N_2^+$, (c) F^-, (d) BF_4^-, (e) FeF_3^-, and (f) FeF_2^-.

DOI: 10.1021/acsami.5b00598
ACS Appl. Mater. Interfaces 2015, 7, 8592–8600

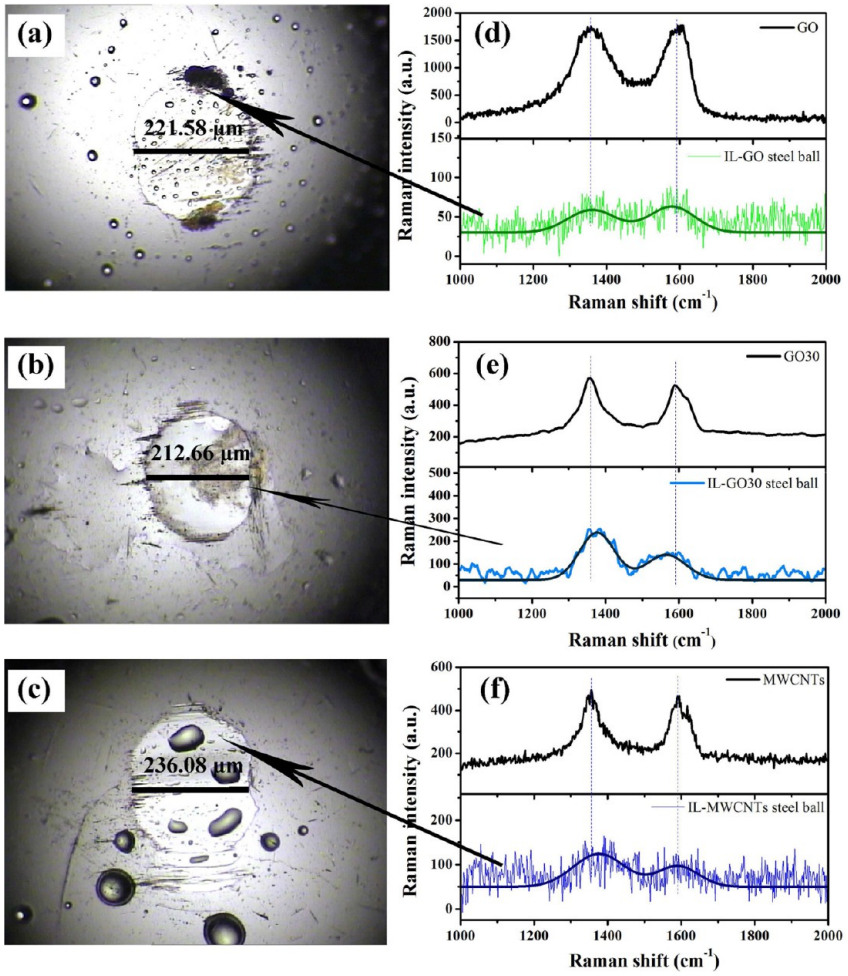

Figure 9. Optical micrographs of wear scar of steel balls after 1 h of friction testing at a load of 30 N and a sliding speed of 0.021 m s^{-1}: (a) IL-GO, (b) IL-GO30, (c) IL-MWCNTs. Raman spectra of (d) pristine GO and wear scar of steel ball, (e) pristine GO30 and wear scar of steel ball, (f) pristine MWCNTs and wear scar of steel ball. Part f also shows Raman spectra confirming its presence as a protective coating within the wear scar of steel balls.

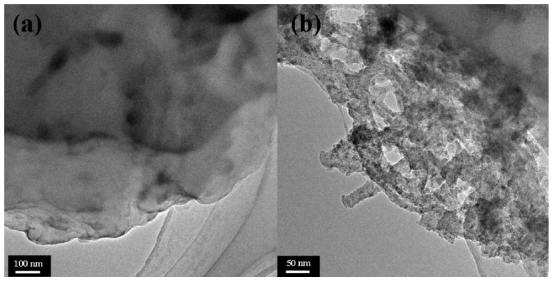

Figure 10. TEM images of the debris: (a) GO after 1 h of friction testing and (b) MWCNTs after 1 h of friction testing. Load: 30 N.

As shown in Figure 12b, parallel graphene layers at a variable distance are stabilized by MWCNTs placed parallel to the graphene planes. In this way, MWCNTs support the graphene layers like pillars and prevent assembly between the graphene layers. Thus, the tribological properties should benefit from the three-dimensional (3D) structure of the hybrid nanoadditives. In particular, graphene sheets stack upon each other and show no effective uniform coverage on the tribofilm surface; thus, the performance of graphene sheets significantly suffers.

The addition of any kind of GO/MWCNT composites (GO30, GO50, or GO70) to the ILs resulted in an improved

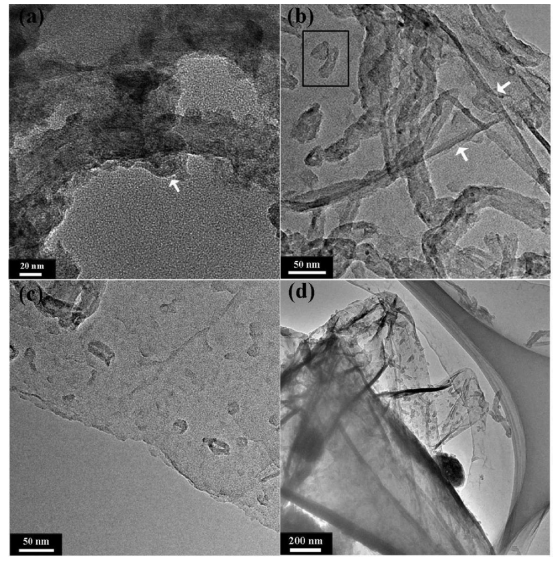

Figure 11. TEM images of the debris of GO30 after 1 h of friction testing: (a) MWCNTs, (b–d) GO and MWCNTs. Load: 30 N.

friction reduction compared to those of the IL-GO (low applied load) and IL-MWCNTs (high applied load, Figure 1); however,

DOI: 10.1021/acsami.5b00598
ACS Appl. Mater. Interfaces 2015, 7, 8592–8600

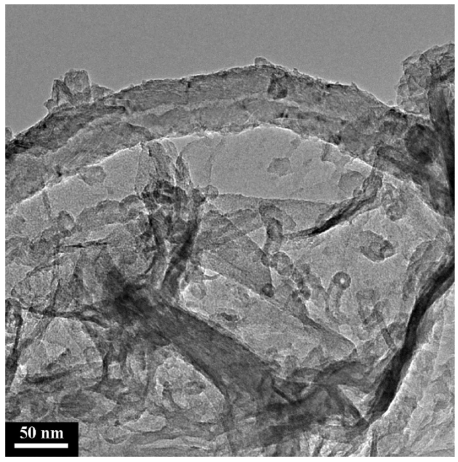

Figure 12. TEM images of the debris of GO30 after 1 h of friction testing. Load: 10 N.

this improvement was influenced by the ratio of GO/MWCNTs. In contrast to that of IL-GO30, the friction levels of IL-GO50 and IL-GO70 are not low and stable. So, a better synergistic effect was observed for friction measurements where the composites with the MWCNTs:GO ratio of 70:30 showed the lowest friction coefficient and lowest wear rate. It was indicated that there was an optimum dose of graphene dissolved into IL. If excess GO was added into ILs, GO would tend to form irreversible agglomerates, and it could not stably and homogeneously disperse in ILs. Both added GO and MWCNTs can avoid this situation. Yang et al.[16] have proposed that the CNTs seem to have effectively reduced the $\pi-\pi$ stacking and agglomeration in graphene nanoplatelets, and together, they produce better antiwear properties.

As further proof, tests were conducted at higher load of 50 N, and it was found that IL-GO30 still provides better friction and wear properties (see Figure 13). The GO and MWCNTs after

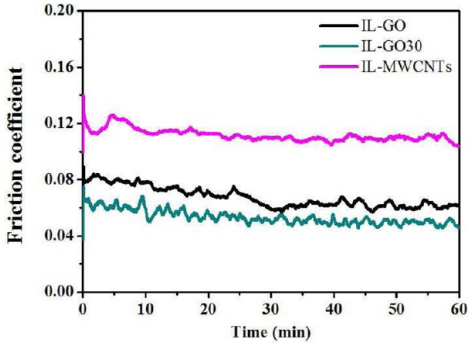

Figure 13. Variations in friction coefficient of IL-GO, IL-GO30, and IL-MWCNTs as a function of sliding time at sliding speed 0.021 m/s. Load: 50 N.

friction testing were observed using a TEM. In the TEM images, MWCNTs were randomly distributed on GO sheets, and some formed aggregates near the edge of GO. The GO nanosheet morphology did not change significantly after the friction testing. In contrast, MWCNTs underwent a dramatic change in morphology after the friction testing. TEM images (Figure 14b,c) revealed a beaded surface on the MWCNTs, with the outer layer of MWCNTs features being increasingly rougher as the load increased. MWCNTs lose much of the initial hollow structure upon the high energy surface strain

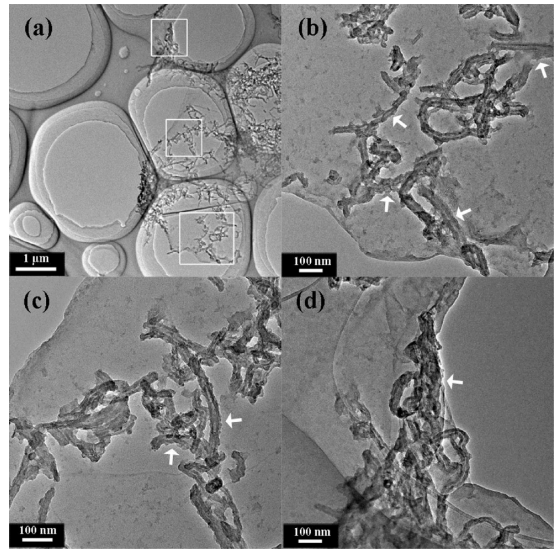

Figure 14. TEM images of the debris: (a) GO and MWCNTs after friction testing at the load of 50 N; (b–d) partial enlargement of part a.

which was produced by the steel balls during the sliding process (see Figure 14d). So, 30GO:70MWCNTs proved to be more effective than single nanoadditive systems.

3.5. Related Wear Mechanisms. The mechanism that governs the tribological properties of the GO and MWCNTs in ILs during friction is proposed on the basis of the results. Figure 15 shows a schematic of the mechanisms of the

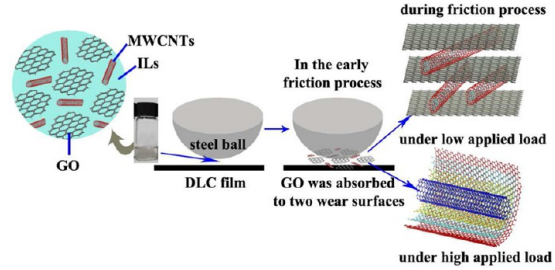

Figure 15. Schematic presentation of friction mechanism under different situation.

DLC/IL/(GO-MWCNTs) composite coatings during friction. The early formation of a GO transfer layer avoids damaging two mating wear surfaces. The friction coefficient is low when only MWCNTs serve as nanoadditives, but the wear rate is higher than with GO-MWCNTs composites acting as nanoadditives. GO layers are easily absorbed on the composite coatings and the counterpart steel ball by sliding toward one direction, which form the early transfer layer before wear debris. During friction, the MWCNTs easily roll between the friction pair, resulting in very low friction coefficients at a low applied load. Under a high applied load, GO layers can form nanobearings between friction pairs, and the tearing and unwrapping of MWCNTs diminish the rolling capability. These deformation mechanisms for individual nanotubes clearly lead to the direct formation of (exfoliated) nanosheets, which can easily adhere to the surface, thereby decreasing the friction coefficient and wear rate.[36] This result can be attributed to the multiwalled structure of the nanotubes. Thus, their synergistic effect considerably enhances IL-GO/MWCNT composites.

DOI: 10.1021/acsami.5b00598
ACS Appl. Mater. Interfaces 2015, 7, 8592–8600

4. CONCLUSION

We demonstrated a simple and effective method to improve friction-reducing and wear-resistance properties in various lubricating states by utilizing GO sheets and MWCNTs as nanoadditives. Through the strong affinity between GO sheets and MWCNTs, excellent dispersion in the ILs was achieved at a GO:MWCNTs weight ratio of ~30:70. A synergistic effect can be established for the hybrid materials by combining 1D MWCNTs and 2D GO films. The composite nanoadditive has great potential for the development of applications in space in the future.

■ ASSOCIATED CONTENT

Supporting Information

Figure S1 showing TEM images of (a) graphene oxide and (b) multiwalled carbon nanotubes. Table S1 showing the contact angle of ILs and five nanofluids. Figure S2 showing UV−vis absorption spectra of ionic liquids with GO or MWCNTs before and after 1 week of storage. Figure S3 showing TG plot of (a) GO and MWCNTs; (b) ILs, IL-GO, and ILMWCNTs. This material is available free of charge via the Internet at http://pubs.acs.org.

■ AUTHOR INFORMATION

Corresponding Author

*Phone: +86-0931-4968080. E-mail: lpwang@licp.cas.cn.

Notes

The authors declare no competing financial interest.

■ ACKNOWLEDGMENTS

This work was supported by the National Natural Science Foundation of China (21373249 and 51322508) and the Nature Science Foundation of Gansu Province of China (Grant 145RJDA329).

■ REFERENCES

(1) Grossman, E.; Gouzman, I. Space Environment Effects on Polymers in Low Earth Orbit. *Nucl. Instrum. Methods Phys. Res., Sect. B* **2003**, *208*, 48−57.

(2) Liu, X.; Wang, L.; Xue, Q. DLC-based Solid−Liquid Synergetic Lubricating Coatings for Improving Tribological Behavior of Boundary Lubricated Surfaces under High Vacuum Condition. *Wear* **2011**, *271*, 889−898.

(3) Sánchez-López, J. C.; Abad, M. D.; Kolodziejczyk, L.; Guerrero, E.; Fernández, A. Surface-Modified Pd and Au Nanoparticles for anti-Wear Applications. *Tribol. Int.* **2011**, *44*, 720−726.

(4) Kang, X.; Wang, B.; Zhu, L.; Zhu, H. Synthesis and Tribological Property Study of Oleic Acid-Modified Copper Sulfide Nanoparticles. *Wear* **2008**, *265*, 150−154.

(5) Lee, K.; Hwang, Y.; Cheong, S.; Kwon, L.; Kim, S.; Lee, J. Performance Evaluation of Nano-Lubricants of Fullerene Nanoparticles in Refrigeration Mineral Oil. *Curr. Appl. Phys.* **2009**, *9*, 128−131.

(6) Liu, Y.; Wang, X.; Pan, G.; Luo, J. A Comparative Study between Graphene Oxide and Diamond Nanoparticles as Water-Based Lubricating Additives. *Sci. China: Technol. Sci.* **2012**, *56*, 152−157.

(7) Rosentsveig, R.; Gorodnev, A.; Feuerstein, N.; Friedman, H.; Zak, A.; Fleischer, N.; Tannous, J.; Dassenoy, F.; Tenne, R. Fullerene-like MoS2 Nanoparticles and Their Tribological Behavior. *Tribol. Lett.* **2009**, *36*, 175−182.

(8) Bhaumik, S.; Prabhu, S.; Singh, K. J. Analysis of Tribological Behavior of Carbon Nanotube Based Industrial Mineral Gear Oil 250cSt Viscosity. *Adv. Tribol.* **2014**, *2014*, 1−8.

(9) Ratoi, M.; Niste, V. B.; Zekonyte, J. WS_2 Nanoparticles-Potential Replacement for ZDDP and Friction Modifier Additives. *RSC Adv.* **2014**, *4*, 21238−21245.

(10) Jatti, V.; Singh, T. P. Copper Oxide Nano-Particles as Friction-Reduction and Anti-Wear Additives in Lubricating Oil. *J. Mech. Sci. Technol.* **2015**, *29*, 793−798.

(11) Ghaednia, H.; Jackson, R. L.; Khodadadi, J. M. Experimental Analysis of Stable CuO Nanoparticle Enhanced Lubricants. *J. Exp. Nanosci.* **2015**, *10*, 1−18.

(12) Eswaraiah, V.; Sankaranarayanan, V.; Ramaprabhu, S. Graphene-based Engine Oil Nanofluids for Tribological Applications. *ACS Appl. Mater. Interfaces* **2011**, *3*, 4221−7.

(13) Khare, V.; Pham, M. Q.; Kumari, N.; Yoon, H. S.; Kim, C. S.; Park, J. I. L.; Ahn, S. H. Graphene−Ionic Liquid Based Hybrid Nanomaterials as Novel Lubricant for Low Friction and Wear. *ACS Appl. Mater. Interfaces* **2013**, *5*, 4063−4075.

(14) Song, H.-J.; Li, N. Frictional Behavior of Oxide Graphene Nanosheets as Water-base Lubricant Additive. *Appl. Phys. A: Mater. Sci. Process.* **2011**, *105*, 827−832.

(15) Lin, J.; Wang, L.; Chen, G. Modification of Graphene Platelets and their Tribological Properties as a Lubricant Additive. *Tribol. Lett.* **2011**, *41*, 209−215.

(16) Yang, S. Y.; Lin, W. N.; Huang, Y. L.; Tien, H. W.; Wang, J. Y.; Ma, C. C. M.; Li, S. M.; Wang, Y. S. Synergetic Effects of Graphene Platelets and Carbon Nanotubes on the Mechanical and Thermal Properties of Epoxy Composites. *Carbon* **2011**, *49*, 793−803.

(17) Artyukh, A. A.; Chernozatonski, L. A.; Sorokin, P. B. Mechanical and Electronic Properties. *Phys. Status Solidi B* **2010**, *247*, 2927−2930.

(18) Lu, X.; Dou, H.; Yuan, C.; Yang, S.; Hao, L.; Zhang, F.; Shen, L.; Zhang, L.; Zhang, X. Polypyrrole/Carbon Nanotube Nanocomposite enhanced the Electrochemical Capacitance of Flexible Graphene Film for Supercapacitors. *J. Power Sources* **2012**, *197*, 319−324.

(19) Yuanqing, L.; Yang, T.; Yu, T.; Zheng, L.; Liao, K. Synergistic Effect of Hybrid Carbon Nantube Graphene Oxide as a Nanofillees in Enhancing the Mechanical Properties of PVA Composites. *J. Mater. Chem.* **2011**, *21*, 10844−10851.

(20) Su, Q.; Liang, Y.; Feng, X.; Mullen, K. Towards Free-Standing Graphene/Carbon Nanotube Composite Films via Acetylene-Assisted Thermolysis of Organocobalt Functionalized Graphene Sheets. *Chem. Commun.* **2010**, *46*, 8279−8281.

(21) Kalin, M.; Zalaznik, M.; Novak, S. Wear and Friction Behaviour of Poly-Ether-Ether-Ketone (PEEK) Filled with Graphene, WS_2 and CNT Nanoparticles. *Wear* **2015**, in press.

(22) Altavilla, C.; Sarno, M.; Ciambelli, P.; Senatore, A.; Petrone, V. New Chimie Douce Approach to the Synthesis of Hybrid Nanosheets of MoS_2 on CNT and Their Anti-Friction and Anti-Wear Properties. *Nanotechnology* **2013**, *24*, 125601−125612.

(23) Lu, L.; Liu, J.; Hu, Y.; Zhang, Y.; Randriamahazaka, H.; Chen, W. Highly Stable Air Working Bimorph Actuator based on a Graphene Nanosheet/Carbon Nanotube Hybrid Electrode. *Adv. Mater.* **2012**, *24*, 4317−4321.

(24) Kim, K.-S.; Shin, B.-K.; Lee, H.; Ziegler, F. Refractive Index and Heat Capacity of 1-Butyl-3-Methylimidazolium Nromide and 1-Butyl-3-Methylimidazolium Tetrafluoroborate, and Vapor Pressure of Binary Systems for 1-Butyl-3-Methylimidazolium Bromide + Trifluoroethanol and 1-Butyl-3-Methylimidazolium Tetrafluoroborate + Trifluoroethanol. *Fluid Phase Equilib.* **2004**, *218*, 215−220.

(25) Suarez, P. A. Z.; Dullius, J. E. L.; Einloft, S.; De Souza, R. F.; Dupont, J. The Use of New Ionic Liquids in Two-Phase Catalytic Hydrogenation Reaction by Rhodium Complexes. *Polyhedron* **1996**, *15*, 1217−1219.

(26) Lal, M.; Singhal, S. K.; Sharma, I.; Mathur, R. B. An Alternative Improved Method for the Homogeneous Dispersion of CNTs in Cu Matrix for the Fabrication of Cu/CNTs Composites. *Appl. Nanosci.* **2013**, *3*, 29−35.

(27) Liu, J.; Rinzler, A. G.; Dai, H.; Hafner, J. H.; Bradley, R. K.; Boul, P. J.; Lu, A.; Iverson, T.; Shelimov, K.; Huffman, C. B.; Rodriguez-Macias, F.; Shon, Y. S.; Lee, T. R.; Colbert, D. T.; Smalley, R. E. Fullerene Pipes. *Science* **1998**, *280*, 1253−1256.

DOI: 10.1021/acsami.5b00598
ACS Appl. Mater. Interfaces 2015, 7, 8592−8600

(28) Liu, X.; Pu, J.; Wang, L.; Xue, Q. Novel DLC/Ionic Liquid/Graphene Nanocomposite Coatings towards High-Vacuum Related Space Applications. *J. Mater. Chem. A* **2013**, *1*, 3797.
(29) Zhang, W.; Zhou, M.; Zhu, H.; Tian, Y.; Wang, K.; Wei, J.; Ji, F.; Li, X.; Li, Z.; Zhang, P.; Wu, D. Tribological Properties of Oleic Acid-Modified Graphene as Lubricant Oil Additives. *J. Phys. D: Appl. Phys.* **2011**, *44*, 205303.
(30) Li, J.; Zhang, C.; Ma, L.; Liu, Y.; Luo, J. Superlubricity Achieved with Mixtures of Acids and Glycerol. *Langmuir* **2012**, *29*, 271−275.
(31) Hamrock, B. J.; Dowson, D. Isothermal Elastohydrodynamic Lubrication of Point Contacts: Part III—Fully Flooded Results. *J. Tribol.* **1977**, *99*, 264−275.
(32) Pensado, A. S.; Comuñas, M. J. P.; Fernández, J. The Pressure−Viscosity Coefficient of Several Ionic Liquids. *Tribol. Lett.* **2008**, *31*, 107−118.
(33) Zeng, X.; Wang, Y.; Wu, X.; Ren, T.; He, Z. Alkyloxy-s-Triazine Derivatives with and without Fluorine-Containing Substituents as Lubricants for Steel−Steel contact. *J. Synth. Lubr.* **2006**, *23*, 1−10.
(34) Lu, R.; Mori, S.; Kobayashi, K.; Nanao, H. Study of Tribochemical Decomposition of Ionic Liquids on a Nascent Steel Surface. *Appl. Surf. Sci.* **2009**, *255*, 8965−8971.
(35) Zhang, L.; Pu, J.; Wang, L.; Xue, Q. Frictional Dependence of Graphene and Carbon Nanotube in Diamond-like Carbon/Ionic Liquids Hybrid Films in Vacuum. *Carbon* **2014**, *80*, 734−745.
(36) Chen, J.; Chen, L.; Zhang, Z.; Li, J.; Wang, L.; Jiang, W. Graphene Layers Produced from Carbon Nanotubes by Friction. *Carbon* **2012**, *50*, 1934−1941.

DOI: 10.1021/acsami.5b00598
ACS Appl. Mater. Interfaces 2015, 7, 8592−8600